JOURNAL OF MATERIALS SCIENCE 31 (1996) 5797–5803

Deformation mechanism in αCu–Al single crystals and bicrystals under scratching with pyramidal indentor

S. KOBAYASHI, M. KUWATA, K. MORI
Department of Mechanical System Engineering, Doshisha University, Tanabe-cho, Tudzuki-gun, Kyoto, 610-03 Japan

S. MIURA
Division of Engineering Physics and Mechanics, Kyoto University, Sakyo-Ku, Kyoto, 606-01 Japan

In order to elucidate the deformation mechanism of materials in abrasive wear process, scratching tests were carried out on the (1 1 1) face of Cu–14.7 at % Al single crystals and Σ13 b bicrystals with pyramidal indentor. In the scratching on the single crystals three kinds of scratching directions, [1 1 $\bar{2}$], [$\bar{1}$ $\bar{1}$ 2] and [$\bar{1}$ 1 0], were chosen. In the case of bicrystals, the [1 $\bar{2}$ 1] and [1 $\bar{1}$ 0] directions were adopted. After scratching the dislocation structure, slip trace patterns and surface profiles across the scratched track were examined. In addition, the dislocation distributions inside the crystals were revealed by successively removing thin layers and developing etch pits on the exposed surface.

The slip traces on either side of the scratched track are produced more extensively than those around the indented point. These slip traces are observed only in the surface of about 100 μm deep, and are not observed in the deeper area. It is found that the microscopic deformations produced due to the scratching consist of three kinds of deformation: formed by indentation, formed by both normal and frictional stresses in the surface layer and formed by stress which is caused in certain limited depth.

The swells of the material were produced in the front of the indentor due to the slips on the {1 1 1} crystal faces which are arranged so as to be diverging into the inside. The azimuths of formation of the swells are [1 1 $\bar{2}$] and [$\bar{2}$ 1 1] in the [1 1 $\bar{2}$] and [$\bar{1}$ 1 0] scratching respectively and [1 $\bar{2}$ 1], [$\bar{2}$ 1 1] in the [$\bar{1}$ $\bar{1}$ 2] scratching.

In the scratching of the bicrystal, the propagation of dislocation in the surface layer of the one side crystal is obstructed by the grain boundary. The microscopic deformation range on the dislocation order is affected by the distribution density of the grain boundaries.

1. Introduction

In order to elucidate the mechanism of wear, it is necessary to acquire knowledge of microscopic deformation produced in the materials on the grain size order, because the wear debris scattering from contacting surface of the general machine elements are of small size order similar to the grain size. For this purpose it is effective to investigate the mechanism of the dislocations and slips caused by friction or scratching in the single crystal grain or grain boundary from microscopic viewpoint. From this point of view, studies on the microscopic deformations caused by friction in regard to single crystals have been performed. Bailey and co-workers have reported the damage on the (0 0 1) and (1 1 1) faces of Cu single crystals scratched with a sapphire ball in air [1]. Steijn discussed an anisotropy of frictional damage using various different materials [2]. Barquins and colleagues have analysed the surface deformation in the case where sapphire ball was scratched on the (1 1 1) face of Cu single crystals [3]. However, in these studies observations were done only on the scratched surface. Before now few studies on the dislocation produced by friction inside the crystal have been done. The authors have reported the dislocation structures produced by indentation and scratching with a spherical indentor on the surface and in the inside of the Cu–Al single crystals [4, 5].

In the present study, in order to examine the dislocation structures and slip traces in the crystal produced by scratching, especially to investigate the effects of the grain boundary, scratching tests were carried out on the surfaces of single crystals and bicrystals.

In the experiments, Cu–Al alloy single crystals and bicrystals with a symmetrical ⟨1 1 1⟩ (27.8°/Σ 13 b) tilt grain boundary were used. The experimental results obtained in the present investigation are effective to

0022–2461

estimate the fundamental mechanism of the crystallographic change in the material prior to wear in the actual machine elements.

2. Test pieces and experimental procedure

Single crystals and bicrystals with a symmetrical ⟨1 1 1⟩ (27.8°/Σ 13 b) tilt grain boundary were used in this study. The test specimens were grown from Cu–14.7 at % Al alloys by the Bridgman technique with increasing speed of the furnace: 30 mm h^{-1} in an atmosphere of 6.665×10^{-3} Pa. The orientation of the crystal face of the specimen was analysed by the X-ray reflecting Laue method. A thin parallelepiped with dimensions of $4 \times 10 \times 20$ mm was cut out from the single crystal block using electrical discharge machining. One of its faces was the (1 1 1) face. Again it was checked using the X-ray method. The accuracy of the cutting was within $\pm 0.5°$ in the gradient of the face. The deviation angle of the crystallographic azimuth between each crystal (Brandon's tolerable error [6]) was within 4.16°. In addition, the specimens were sealed in an evacuated quartz tube at 6.665×10^{-3} Pa and annealed for 50 h in the temperature range 750–950 °C. After annealing, the crystal face of the specimen was polished mechanically and electrolytically to remove the oxide layer and to obtain a mirror-finished surface. A Vickers' quadrangular pyramid indentor was used for the scratching test. The indentor was statically indented on to the (1 1 1) face for 30 s, orienting its diagonals to the [1 1 $\bar{2}$] direction and was scratched with a constant feeding speed of 0.5 mm s^{-1} under a load of 10.0 N. Three scratching directions [1 1 $\bar{2}$], [$\bar{1}$ $\bar{1}$ 2] and [$\bar{1}$ 1 0] were adopted.

With the bicrystals, the scratching was made in the [1 $\bar{1}$ 0] or reverse [$\bar{1}$ 1 0] direction in one single crystal as shown in Fig. 1. In this case the other crystal was scratched in the [1 $\bar{2}$ 1] or [$\bar{1}$ 2 $\bar{1}$] direction, respectively.

The distributions of slip traces produced by scratching were observed with an optical microscope. The surface was etched using the etchant shown in Table I to examine the dislocation structures. In addition, the dislocation structures inside the crystals were revealed for every removal of surface layer of 10 μm thickness with the electrolytic solution, the composition of which is shown in Table II.

TABLE I Composition of etchant (mol)

HCl	CH_3COOH	Br	H_2O
3.4	2.0	0.43	5.5

TABLE II Composition of solution used in electrolytic polishing (mol)

H_3PO_4	C_2H_5OH	$CH_3CH_2CH_2OH$	NH_2CONH_2
11	3.3	0.51	0.26

3. Experimental results and discussions

3.1. Deformation in single crystals

3.1.1. Scratching in the [1 1 $\bar{2}$] direction

Fig. 2 shows the appearance of deformation on the (1 1 1) face of the single crystal after scratching in the [1 1 $\bar{2}$] direction. Fig. 3 shows the sketch diagram of this appearance. This sketch diagram was described while observing the scratched surface with the

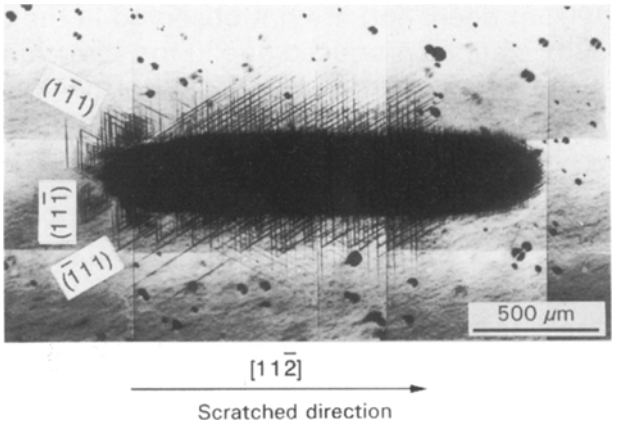

Figure 2 Appearance of deformation on scratched surface after scratching in [1 1 $\bar{2}$] direction.

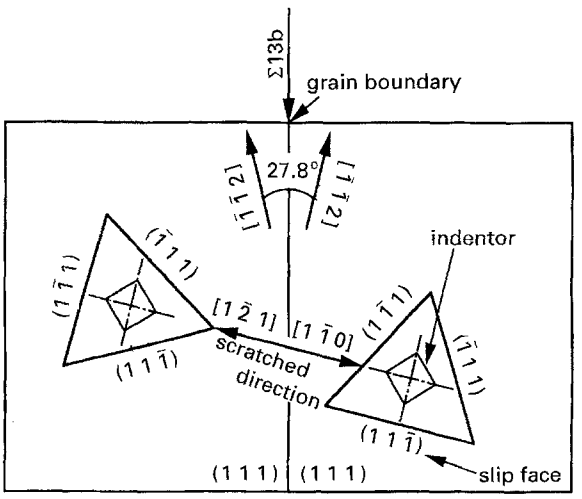

Figure 1 Setting azimuth of indentor and scratched direction on bicrystal.

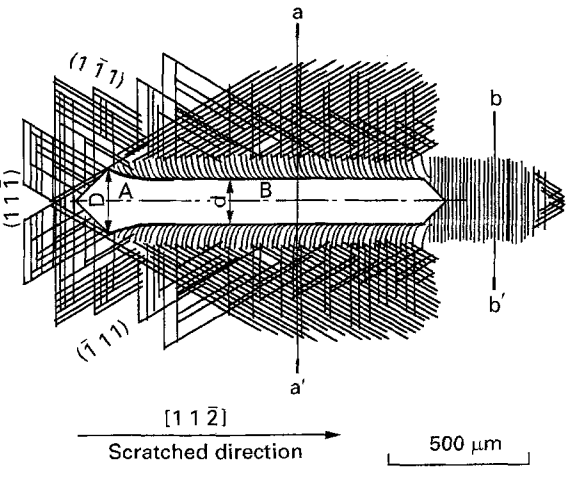

Figure 3 Sketch diagram of scratched track and slip traces.

microscope, as the fine slip traces and the scratched track which are not clear in Fig. 2 can be observed clearly. The width of the indented area D at the point A before scratching is about 230 μm, while the width of the scratched track d at the position B is narrower than D, and is about 160 μm. The slip traces are produced on either side of the scratched track by slip deformations on the $(1\,1\,\bar{1})$, $(1\,\bar{1}\,1)$ and $(\bar{1}\,1\,1)$ faces intersecting the scratched surface. The deformed area is extended in the distance of 500–530 μm from the centre of the scratched track. This value is larger than 400–420 μm which was recorded at the indented point. Fig. 4 shows the surface profiles recorded along the lines a–a′ and b–b′ shown in Fig. 3. As shown in Fig. 4(a), the swells of which maximum height is about 5 μm are produced in the range of about 300 μm width on both sides of scratched track. And as shown in Fig. 4(b), the mountain-shaped swelling of width about 450 μm spreads over about 400 μm in the front area of scratched track. These swellings are caused by slips on the $(1\,1\,\bar{1})$ face due to the frictional force accompanying so-called dig-out shearing stresses. In addition, the slip traces on the $(1\,\bar{1}\,1)$ and $(\bar{1}\,1\,1)$ faces are produced in front of these swells. It is considered that these slip traces are produced to ease the swelling deformation on the $(1\,1\,\bar{1})$ face. These three slip faces are arranged so as to diverge downwards from each other. An indentor scratches through such a deformed and strain hardened area, so the width of scratched track is reduced compared as the width of the deformed area at indented point. Fig. 5(a) shows the appearance of the dislocation structure around the scratched track. Fig. 5(b), (c) and (d) show the dislocation structures on the faces at 60, 300 and 400 μm depth respectively. The arrangements of the dislocations produced around the scratched track are shown in Fig. 5(a) and (b). The swelling caused by slips on the $(1\,1\,\bar{1})$ face in the front area of the scratched track are observed (as shown in Fig. 5(b)) with a mark ①. Slip traces with these swellings are observed only in the surface layer about 100 μm deep, and are not observed in Fig. 5(c) and (d). It is considered that the remaining slip traces observed on either side of the scratched track at the depth of 300 and 400 μm are mainly caused by the normal component of the stresses due to the scratching force. The dislocation density around the scratched track decreases equally at the depth of 60 μm as compared with that on the surface. The slip traces observed at 300 μm depth are very small in number and scarcely expand on either side of the track. At this depth, the width of the deformed area at the indented point is nearly equal to that in the scratched track area. This fact indicates that the deformation inside the crystal is mainly produced due to the normal component of the stress rather than the frictional component parallel to the surface. From these experimental results, the plastic deformations produced by scratching are considered to be formed with three areas of deformation, as shown schematically in Fig. 6, i.e. the region A formed by indentation, B formed by normal and frictional stresses in the

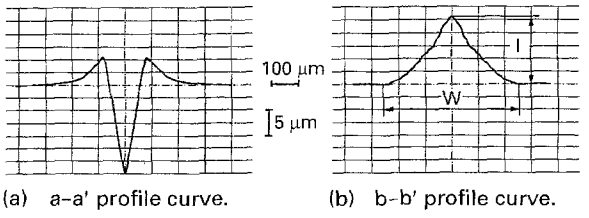

Figure 4 Surface profile curves across scratched track.

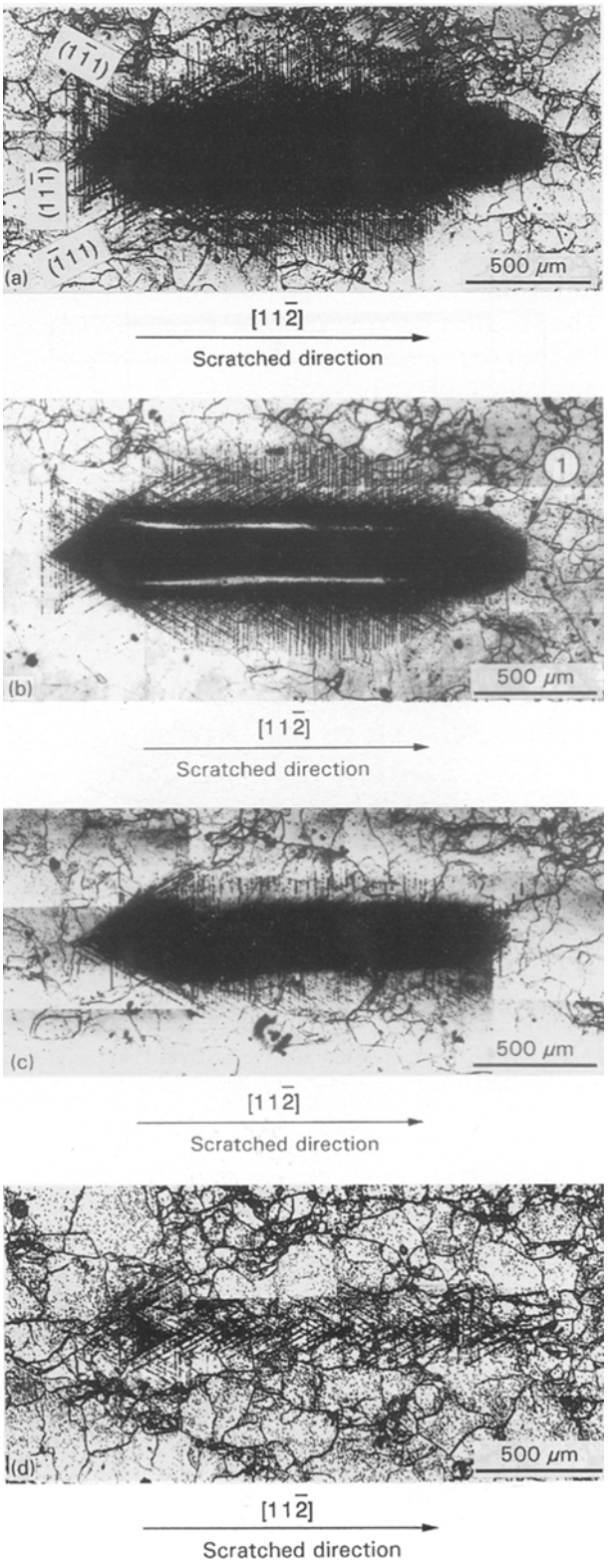

Figure 5 Appearances of etch pits distributions after scratching in $[1\,1\,\bar{2}]$ direction. (a) Dislocation structure at surface level. (b) Dislocation structure at 60 μm depth. (c) Dislocation structure at 300 μm depth. (d) Dislocation structure at 400 μm depth.

surface layers and C formed by the normal stress component in the deeper area than B.

3.1.2. Deformations in the [$\bar{1}\,\bar{1}\,2$] scratching

Figs 7 and 8 show the appearance of the deformation after scratching in the [$\bar{1}\,\bar{1}\,2$] direction and its sketch diagram of this appearance, respectively. Fig. 9 shows

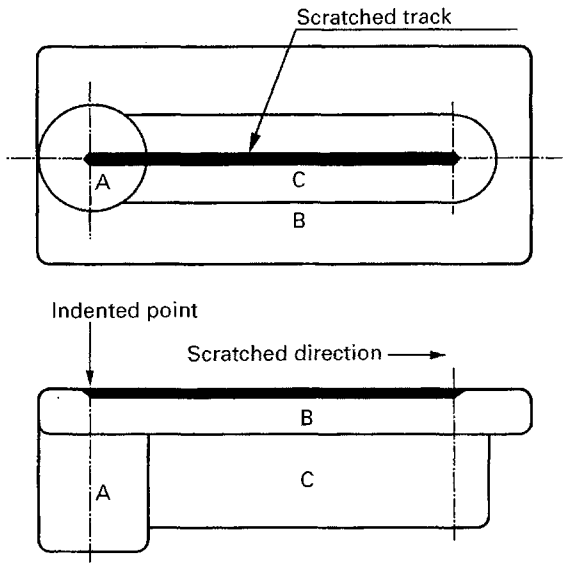

Figure 6 Plastically deformed region produced by scratching on (1 1 1) surface.

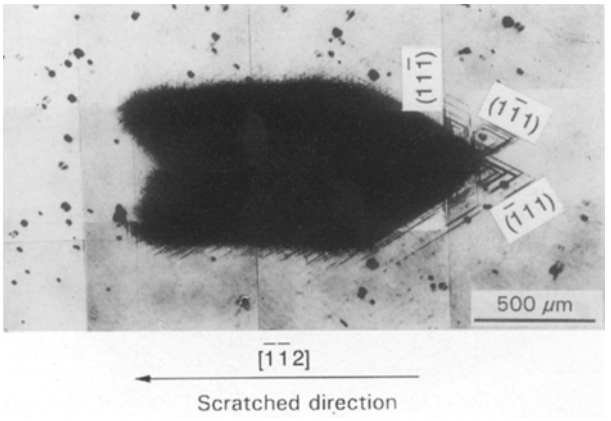

Figure 7 Appearance of deformation on scratched after scratching in [$\bar{1}\,\bar{1}\,2$] direction.

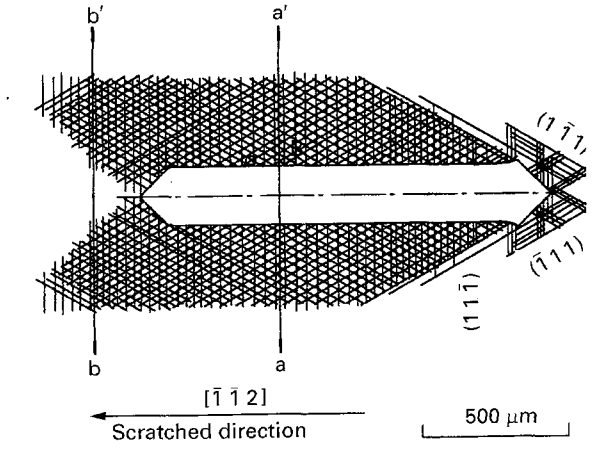

Figure 8 Sketch diagram of scratched track and slip traces.

the surface profiles across the track recorded in the same way as that shown in Fig. 4. The slip traces on either side of the track are more densely distributed than those observed in the [1 1 $\bar{2}$] scratching. The swelling are observed in the front area of the scratched track, i.e. in the [1 1 $\bar{2}$] azimuth in the [1 1 $\bar{2}$] scratching, whereas they are separately produced in [$\bar{2}$ 1 1] and [1 $\bar{2}$ 1] azimuths in the [$\bar{1}\,\bar{1}$ 2] scratching. These swellings are caused due to the slips on the ($\bar{1}$ 1 1) face on the right side and on the (1 $\bar{1}$ 1) face on the left side of scratched track respectively. Comparing Fig. 4(a) with Fig. 9(a), the width W and maximum height H of the swollen region increase by approximately 1.7 and 2.5 times those in the [$\bar{1}\,\bar{1}$ 2] scratching respectively. Comparing Fig. 4(b) with Fig. 9(b), the height of the swelling in front of the scratched track is about 0.6 times as large as that in the [$\bar{1}\,\bar{1}$ 2] scratching. Such deformed regions are strain-hardened due to the scratching and restrain the deformations in the side area of the track. This tendency is remarkable in the [$\bar{1}\,\bar{1}$ 2] scratching as compared with the case of the [1 1 $\bar{2}$] scratching. For this reason, the magnitude of the microscopic deformations in the track sides are smaller than in the indented area as obtained in the present experimental results. In the [$\bar{1}\,\bar{1}$ 2] scratching in which such swellings remarkably appear, the width of the scratched track on the surface is wider than that in the [1 1 $\bar{2}$] scratching.

3.1.3. Deformations in the ⟨1 1 0⟩ scratching

Figs 10 and 11 show the appearance of the deformation after scratching in [$\bar{1}$ 1 0] direction and its sketch diagram respectively. Fig. 12 shows surface profiles recorded on a–a′ and b–b′ lines shown in Fig. 11. The width of the scratched track is about 180 μm, and it is a middle value between 160 μm in the [1 1 $\bar{2}$] scratching

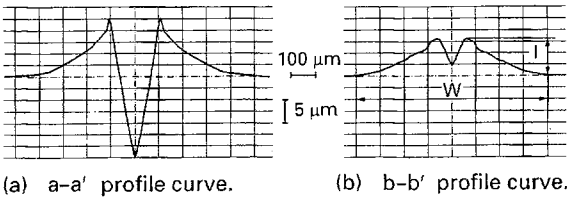

Figure 9 Surface profile curves across scratched track.

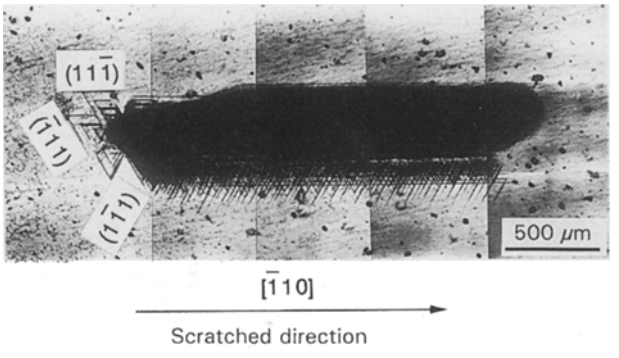

Figure 10 Appearance of deformation on scratched surface after scratching in [$\bar{1}$ 1 0] direction.

and 210 μm in the $[\bar{1}\,\bar{1}\,2]$ scratching. On the left side of the track, the distribution of the slip traces due to the slips on the $\{1\,1\,1\}$ faces is denser than those in the $[1\,1\,\bar{2}]$ and $[\bar{1}\,\bar{1}\,2]$ scratchings, but is comparatively sparse on the right side. The deformed region on the right side is more extensive than on the left side, and extends over 400 μm from the scratched track. The swelling extends to about 350 μm on the left side of the scratched track as shown in Fig. 12(a). The maximum height of the swelling is 13 μm. This is also a middle value between the case of the $[1\,1\,\bar{2}]$ and $[\bar{1}\,\bar{1}\,2]$ scratchings. The swelling has a gentle slope on the right side and its maximum height is only 2 μm. The swelling in front of the scratched track is mainly produced in the $[\bar{2}\,1\,1]$ azimuth, i.e. on the left side of the scratched track. This indicates that the slips on the $(\bar{1}\,1\,1)$ faces occur in this region. As described above, the swellings are produced in front of the scratched track in the $[1\,1\,\bar{2}]$ scratching, and on both side areas in the $[\bar{1}\,\bar{1}\,2]$ scratching, and only on the left side of the scratched track in the $[\bar{1}\,1\,0]$ scratching. Consequently, the extent of the deformation to the left side is suppressed, and the deformed region is smaller on the left side than on the right side. Also the dislocation rows extend over 400 μm in the front area of the track, but these dislocations do not spread over 100 μm beneath the track. Namely, the region of the plastic deformation in the $[\bar{1}\,1\,0]$ scratching is decided by these widths and depths. Such a region of the deformation in the surface layer is widest in the $[1\,1\,\bar{2}]$ scratching among the three kinds of directional scratchings. The deformation of the surface layer is more restrained in the $[\bar{1}\,1\,0]$ scratching than in the $[1\,1\,\bar{2}]$ scratching. The effect of the scratching in the direction of the depth is most prominent in the $[\bar{1}\,\bar{1}\,2]$ scratching. As compared with this, in the $[1\,1\,\bar{2}]$ scratching, the slip deformations on the $\{1\,1\,1\}$ face are clearly produced in the azimuth of the moving indentor, and the effects on the deformation in the inside of the crystals are comparatively small.

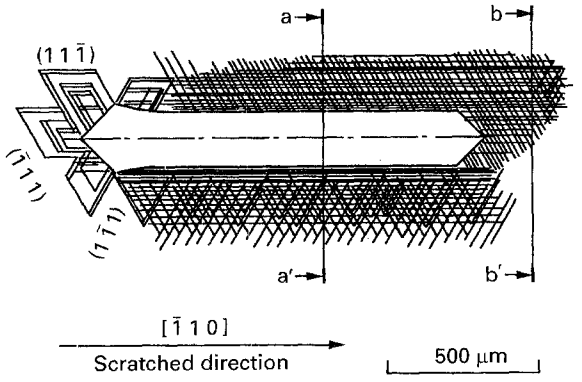

Figure 11 Sketch diagram of scratched track and slip traces.

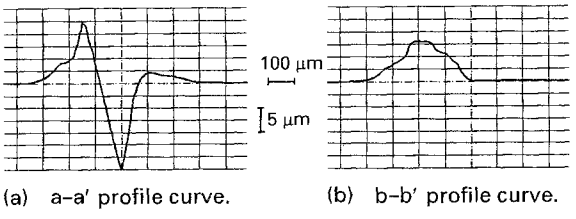

Figure 12 Surface profile curves across scratched track.

3.2. Deformation of bicrystals

Fig. 13 shows the appearance of the deformation in Σ13b bicrystals after scratching in the direction shown in Fig. 1. Fig. 14 shows the sketch diagram of this appearance. In this case, scratched directions are the $[1\,\bar{1}\,0]$ in the crystal Ⓘ given the start of the scratching, and $[\bar{1}\,2\,1]$ in the other crystal Ⓘⓘ. The deformation pattern in the region at over 100 μm distance from the grain boundary shows the same pattern as that in the case of scratching given to a single crystal in the $[\bar{1}\,1\,0]$ direction. The deformation pattern in the other crystal at the same distance from the grain boundary is also the same pattern as that observed in the $[1\,1\,\bar{2}]$ directional scratching of the single crystal. The width of the scratched track in the neighbourhood of the grain boundary (cf. mark A) is about 140 μm, and this value is slightly smaller than 160 μm, observed in the other area. Such a difference in the width of the track is considered to be for the following reason. Dislocations in the crystal Ⓘ are interpreted around the grain boundary and the strain hardening is caused by pile-up of these dislocations, so

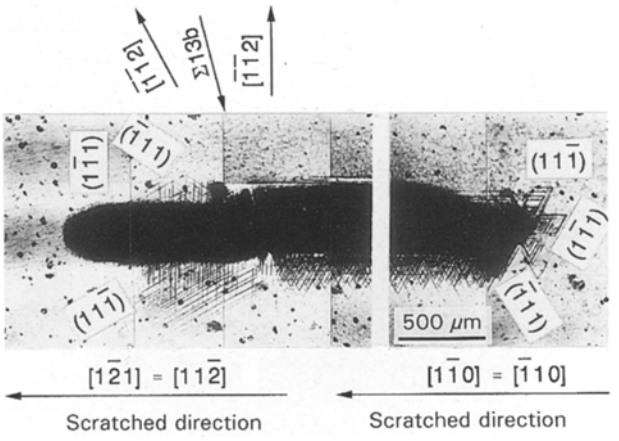

Figure 13 Appearances of deformation on scratched bicrystal. (Scratched direction: right crystal $[1\,\bar{1}\,0]$, left crystal $[1\,\bar{2}\,1]$).

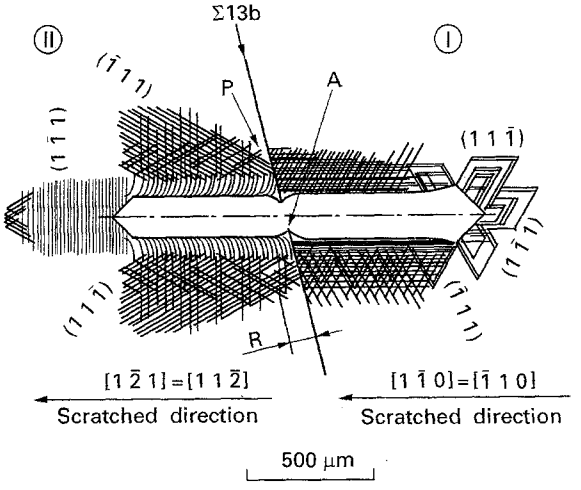

Figure 14 Sketch diagram of scratched track and slip traces.

the deformations are restrained as the result. It is found that the deformation scarcely extends into the area P near the boundary of the crystal Ⅱ due to these pile-ups of the dislocations. The effect of the grain boundary on the width of the scratched track and the slip traces extends in a range of R and is limited with the distance 80 ~100 μm from the grain boundary. It is confirmed that the deformations on the etched surface shown in Fig. 15(a) have been influenced by existence of the grain boundary. However, the deformation patterns inside the crystal around the grain boundary shown in Fig. 15(b), (c) and (d) show just the same patterns as those in the case of scratching of the single crystals, and two kinds of deformation are joined to each other in the neighbourhood of grain boundary. This result indicates that the effects of the frictional force on the deformation are limited only in the surface layer and the deformation inside of the crystal is produced by the stresses acting normally to the specimen surface. In other words, in the scratching across the grain boundary, the propagations of the deformation in the surface layer of one side crystal are obstructed by the grain boundary, and the degree of deformation of the other side crystal is affected by this restrain. However, the comparatively small deformation produced in the inside of the crystal is little influenced by grain boundary. As mentioned above, the deformations inside the crystal of the bicrystals are reduced to domination by the slip systems of each crystal.

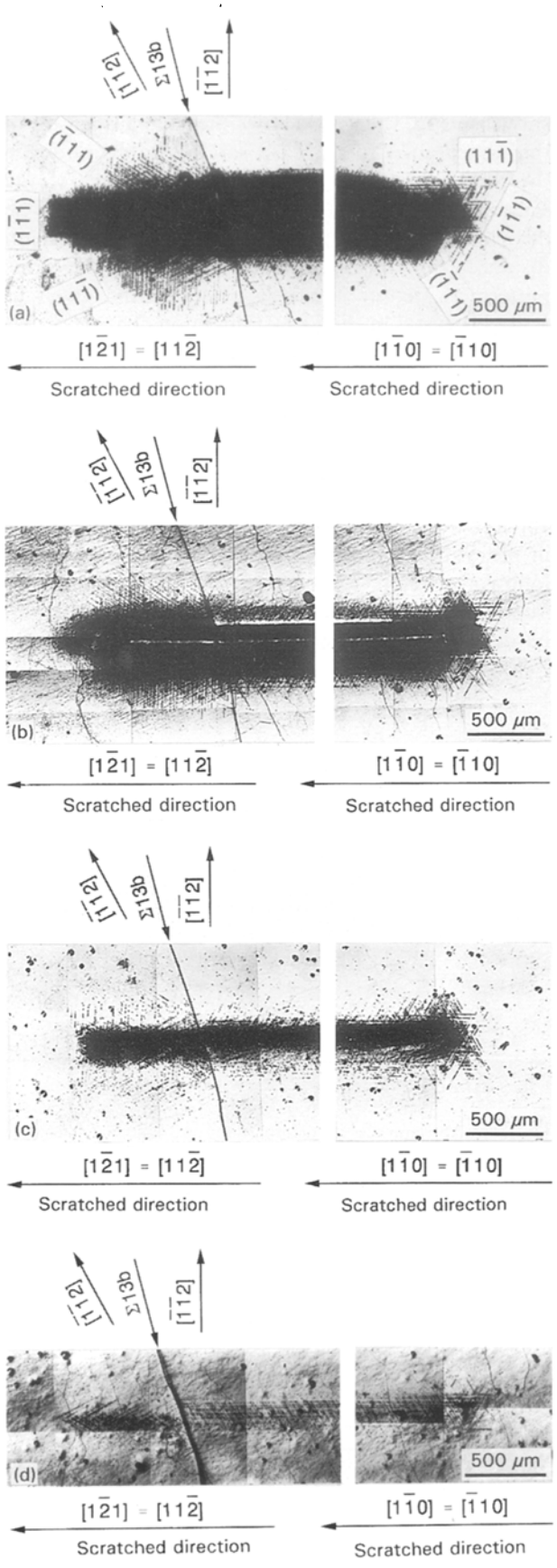

Figure 15 Appearances of etch pits distributions on scratched bicrystal surface. (a) Dislocation structure at surface level. (b) Dislocation structure at 100 μm depth. (c) Dislocation structure at 300 μm depth. (d) Dislocation structure at 500 μm depth.

Fig. 16 shows the appearance of the deformation on the surface of the Σ13 b bicrystals after scratching in the [$\bar{1}$ 1 0] direction. Fig. 17 shows the sketch diagram of this appearance. Also in this case, in the region far from the grain boundary, the same deformations as those observed under single crystal scratching in the equivalent direction are respectively produced. The width of the scratched track across the grain boundary is about 160 μm, and its value is also smaller than that observed in the area a short distance away from the grain boundary. The effects of the grain boundary to the formation of the scratched track and the slip traces are probably limited around the grain boundary in the case of the [1 $\bar{1}$ 0] scratching.

From the experimental results on the bicrystals, it has been clarified that in the scratching across the grain boundary with a sharp shaped indentor as used in the present study, the slip traces show a different

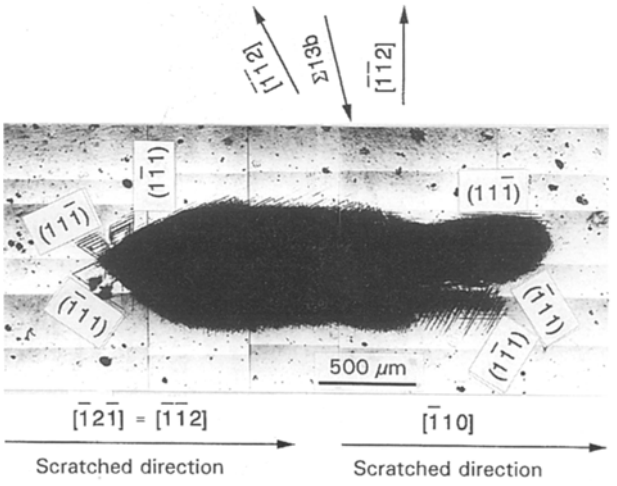

Figure 16 Appearance of deformation on scratched bicrystal. (Scratched direction: right crystal [$\bar{1}$ 1 0], left crystal [$\bar{1}$ 2 $\bar{1}$])

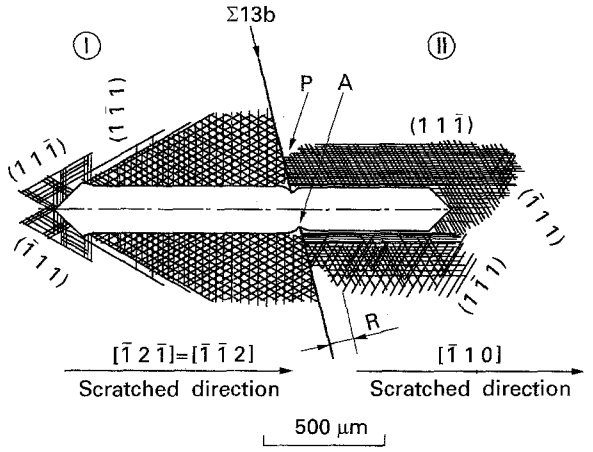

Figure 17 Sketch diagram of scratched track and slip traces.

distribution pattern which corresponds to the crystal orientation, and that the width of the scratched track and the pattern of the slip traces are influenced by the dislocations accumulated around the boundary. However, the range in which such influence extends is relatively small under the experimental conditions of 10.0 N loading used in the present study, and the whole deformation pattern is not greatly influenced by the grain boundary. The dislocations propagate through the grain boundary in the polycrystal material. When the dislocations are relatively small, the propagations are restrained at the grain boundary. Therefore, microscopic plastic deformation of the dislocation order is greatly affected by the distribution density of the grain boundaries and the crystal grain size.

4. Conclusions

In order to elucidate the mechanism of microscopic deformation in the scratching, the scratching tests were carried out on the (1 1 1) face of αCu–Al single crystals and Σ13b bicrystals with pyramidal indentor. The conclusions obtained are summarized as follows.

1. The slip traces on either side of the scratched track are produced more extensively than those around the indented point. The swellings of the material were caused in the front area of the indentor due to the slips on the {1 1 1} crystal faces which are arranged in divergent form into the inside. So, the width of the scratched track in scratched area becomes narrower than that at the indented point.
2. The azimuths of formation of the swellings are [1 1 $\bar{2}$] in the [1 1 $\bar{2}$] scratching, [1 $\bar{2}$ 1] and [$\bar{2}$ 1 1] in the [$\bar{1}$ $\bar{1}$ 2] scratching and [$\bar{2}$ 1 1] in the [$\bar{1}$ 1 0] scratching. Ranges of the deformations in the surface layer and inside the crystal are influenced by this azimuth. The range of the deformation in the surface layer is greater in the [1 1 $\bar{2}$] scratching than in the [$\bar{1}$ $\bar{1}$ 2] scratching. The scratched direction which produces the greatest deformations in the inside of the crystal is the [1 1 $\bar{2}$], and the smallest in the [$\bar{1}$ $\bar{1}$ 2] scratching.
3. The microscopic deformations produced due to the scratching consist of three kinds of deformation: formed by indentation, formed by both normal and frictional stresses of the surface layer and formed by stress which is caused at certain limited depth.
4. In the scratching of the bicrystal, the propagation dislocation in the surface layer of the one side crystal is obstructed by the grain boundary. However, the deformation inside the crystal is little affected and is dominated by the peculiar slip systems of each crystal. Microscopic deformation range on the dislocation order is affected by the distribution density of the grain boundaries.

References

1. T. M. BAILEY and A. T. GWATHMAY, *ASLE Trans.* **5** (1962) 45.
2. R. P. STEIJN, *Wear* **7** (1962) 48.
3. M. BARQUINS, M. KENNEL and R. COURTEL, *ibid.* **11** (1968) 87.
4. S. KOBAYASHI, T. HARADA and S. MIURA, *J. Mater. Sci.* **26** (1991) 3945.
5. S. KOBAYASHI, T. HATAKEYAMA and S. MIURA, *J. Soc. Mater. Sci. Japan* **39** (1990) 1663.
6. D. G. BRANDON, *Acta. Metall.* **14** (1966) 1479.

Received 14 September 1994
and accepted 7 November 1995